Title

3D printing based on cardiac CT assists anatomic visualization prior to transcatheter aortic valve replacement

Journal

Journal of Cardiovascular Computed Tomography, 10(1)

ISSN

1934-5925

Authors

Ripley, Beth
Kelil, Tatiana
Cheezum, Michael K
et al.

Publication Date

2016

DOI

10.1016/j.jcct.2015.12.004

Peer reviewed

HHS Public Access

Author manuscript

J Cardiovasc Comput Tomogr. Author manuscript; available in PMC 2017 August 28.

Published in final edited form as:

J Cardiovasc Comput Tomogr. 2016 ; 10(1): 28–36. doi:10.1016/j.jcct.2015.12.004.

3D Printing Based on Cardiac CT Assists Anatomic Visualization Prior to Transcatheter Aortic Valve Replacement

Beth Ripley, MD, PhD[1,5], **Tatiana Kelil, MD**[1], **Michael K. Cheezum, MD**[1,2], **Alexandra Goncalves, MD, PhD**[2,3], **Marcelo F. Di Carli, MD**[1,2], **Frank J. Rybicki, MD, PhD**[4], **Mike Steigner, MD**[1], **Dimitrios Mitsouras, PhD**[1], and **Ron Blankstein, MD**[1,2]

[1]Department of Radiology, Brigham and Women's Hospital, Harvard Medical School, Boston, MA

[2]Department of Medicine (Cardiovascular Division), Brigham and Women's Hospital, Harvard Medical School, Boston, MA

[3]University of Porto Medical School, Porto, Portugal

[4]The Ottawa Hospital Research Institute and Department of Radiology, The University of Ottawa, Ottawa, ON, Canada

Abstract

Background—3D printing is a promising technique that may have applications in medicine, and there is expanding interest in the use of patient-specific 3D models to guide surgical interventions.

Objective—To determine the feasibility of using cardiac CT to print individual models of the aortic root complex for transcatheter aortic valve replacement (TAVR) planning as well as to determine the ability to predict paravalvular aortic regurgitation (PAR).

Methods—This retrospective study included 16 patients (9 with PAR identified on blinded interpretation of post-procedure trans-thoracic echocardiography and 7 age, sex, and valve size-matched controls with no PAR). 3D printed models of the aortic root were created from pre-TAVR cardiac computed tomography data. These models were fitted with printed valves and predictions regarding post-implant PAR were made using a light transmission test.

Results—Aortic root 3D models were highly accurate, with excellent agreement between annulus measurements made on 3D models and those made on corresponding 2D data (mean difference of −0.34 mm, 95% limits of agreement: ± 1.3 mm). The 3D printed valve models were within 0.1 mm of their designed dimensions. Examination of the fit of valves within patient-specific aortic root models correctly predicted PAR in 6 of 9 patients (6 true positive, 3 false negative) and absence of PAR in 5 of 7 patients (5 true negative, 2 false positive).

Address for Correspondence: Ron Blankstein, M.D., F.A.C.C., Non-Invasive Cardiovascular Imaging Program, Departments of Radiology and Medicine (Cardiovascular Division), Brigham and Women's Hospital; 75 Francis St, Boston MA, 02115, USA rblankstein@partners.org, Phone (857) 307-1989; Fax (857) 307-1955.

[5]Present Address: Department of Radiology, University of Washington, Seattle, WA

The authors have no conflicts of interest

Conclusions—Pre-TAVR 3D-printing based on cardiac CT provides a unique patient-specific method to assess the physical interplay of the aortic root and implanted valves. With additional optimization, 3D models may complement traditional techniques used for predicting which patients are more likely to develop PAR.

Keywords

3D printing; 3-D printing; 3-dimensional; additive manufacturing; TAVR; aortic valve; paravalvular leak; paraoartic regurgitation

Introduction

Transcatheter aortic valve replacement (TAVR) utilizes a catheter-based delivery system to deliver a prosthetic valve mounted within a stent into a diseased aortic valve. While TAVR is a safe alternative to surgery in appropriately selected patients with aortic stenosis[1], there are known limitations. For instance, there is no direct access to the patient's anatomy to provide precise prosthesis sizing and the complex 3-dimensional anatomy of the aortic root makes it difficult to predict how the prosthetic valve will adapt in situ. [2] Moreover, the prosthetic valve is secured at the annular plane in a sutureless fashion and failure to achieve a circumferential seal can result in paravalvular aortic regurgitation (PAR). [3] PAR is the most frequent complication after TAVR and carries increased morbidity and mortality. [4, 5] Therefore, meticulous pre-procedural imaging with transthoracic echocardiography (TTE), transesophageal echocardiography (TEE), and/or cardiac computed tomography (cardiac CT) is required to ensure the most optimal fit.

Three-dimensional (3D) printing can provide personalized models of patient- specific anatomy for pre-surgical planning and surgical device design. To date, 3D printing has been used for pre-procedural planning in a small number of cardiovascular cases involving coronary arteries [6], intracardiac defects [7–9], mitral [10–14] and pulmonic valves [15, 16]. To our knowledge, however, there is no published data regarding the utility of 3D printing to guide TAVR.

In this proof-of-concept study, we aimed to determine whether patient-specific 3D printed models could be used to visualize the fit between the native aortic valve complex and TAVR prosthetic valves, and thus predict the occurrence of post- procedural PAR.

METHODS

Study Population

In a retrospective fashion, we examined 16 patients in whom pre-TAVR cardiac CT and post-TAVR TTE were available (Table 1). Eight patients with clinically documented PAR were initially selected from a larger database based on the following criteria: (1) patients had an ECG-gated pre-procedure CCT with multiphase acquisition to ensure coverage during the systolic phase of the cardiac cycle and (2) they had a follow-up transthoracic echo (TTE) within 1 month of the procedure that demonstrated at least mild PAR. Subsequently, 8 TAVR patients without PAR were matched for age, sex and size of implanted valve.

The presence or absence of PAR on the post-procedure TTE was confirmed by two experienced cardiologists with level III training in echocardiography (M.C. and A.G.), blinded to all patient data. This review led to the reassignment of one control patient (patient 3) to the PAR group based on consensus from both readers, resulting in a final count of 9 patients with PAR and 7 control patients.

All patients in the study received balloon-expandable Edwards Sapien valves (7 Sapien, 4 Sapien XT and 5 Sapien-3; Edwards Life Sciences, Irvine, CA). Prosthesis size was selected based on the annulus diameter, as measured by cardiac CT according to published recommendations [17], and all valves were maximally expanded. Re-ballooning of valves at the time of placement was done at the discretion of the interventionalist.

The study was approved by the Partners Healthcare Institutional Review Board and was conducted in accordance with institutional guidelines.

Pre-Procedural Cardiac CT

All cardiac CT scans were performed by volumetric prospective electrocardiogram-gated acquisition through the heart over a complete R-R interval (0-95% phase), followed by non-gated images of the abdomen and pelvis using a 320×0.5 mm detector row scanner with a gantry rotation time of 350 milliseconds (Toshiba Aquilion One Dynamic Volume CT, Tochigi-ken, Japan). Patients received 50–100 mL of iodinated contrast, followed by 40 mL of normal saline, at a rate of 5–6 mL per second. Contrast bolus tracking was performed in all patients with a region of interest in the descending aorta using a 200 Hounsfield unit threshold. No medications were administered prior to the scan.

Post-Procedural TTE

PAR was evaluated on post-procedural TTE studies using the different parameters indicated in the VARC-2 recommendations and graded based on the Unifying Grading Scheme Proposal. [18] All TTE studies were examined by a consensus read of 2 experienced cardiologists, blinded to all patient data.

Creation of 3D Models and Valves

For each patient, multiphase data sets were reconstructed at 5% intervals across one R-R interval (0-95%) at 0.5 mm slice thickness with 0.25 mm overlap using a medium smooth kernel. The peak systolic phase interval (determined by maximal opening of the aortic valve) was identified and was used for creating the 3D model. The blood pool of the aortic root, annulus and left ventricular outflow tract was segmented using manually determined threshold values adjusted for each patient to include contrast but exclude eccentric calcium. Segmentation was then manually edited to exclude the left atrium and left ventricle (Figure 1) using 3D visualization software (Vitrea 6.7, Vital Images) by a radiologist (B.R.) blinded to TTE findings. Segmented data sets were then converted to a 3D printable standard tessellation language (STL) file and exported into computer aided design software (3-matic, Materialise) for further post-processing. A 2 mm thick wall was added to the outside of the blood pool in all models; this strategy was necessary because the true aortic wall was too thin to segment and printer capabilities required a 2 mm minimum wall thickness. Annular

calcium was accounted for in the models by indentations in the segmented blood pool at the sites of calcium (allowing incorporation of solid material into the model at these sites, figure 1). Valve leaflets were not included in the model since non-calcified portions were too thin to accurately segment and print.

Aortic models were 3D printed using a stereolithography 3D printer (Form 1 plus, Formlabs, Cambridge, MA) and flexible material (clear flexible resin, Formlabs). Valve models meeting Sapien size specifications (23, 26 & 29 mm) but with a modified closed base were designed in 3-matic and printed on a material extrusion 3D printer in hard plastic (Printrbot Metal, Printrbot) (Figure 2).

Accuracy of 3D Models

To confirm that 3D models accurately depicted annulus size, we compared maximum and minimum diameter measurements made on models with calipers to standard annulus measurements made on cardiac CT by two experienced observers. Agreement between the two measurement methods was quantified by Bland Altman plot.

PAR Prediction Test

We devised a simple light test in order to predict PAR (Figure 2). The valve model corresponding in size to each patient's actual implanted prosthesis (23, 26 or 29 mm) was carefully positioned in the individual aortic model at the level of the aortic annulus. The presence of PAR was then determined via projection of light through the left ventricular outflow tract onto a thin film and captured with a digital camera (Figure 2). In cases where the prosthetic valve was well circumscribed by the aortic valve complex, the majority of light was blocked by the closed valve and only faint background light in the shape of the annulus and proximal LVOT was projected onto the thin film. In cases where gaps existed between the aortic wall and the valve, transmitted light was projected onto a thin film in a bright crescent. The presence of PAR (binary decision defined as any paravalvular light transmission) was made by consensus of 2 readers blinded to TTE results (B.R. and D.M.). The position of PAR was recorded based on the clock face position, as described by Goncalves et al. [19]

Quantification of Predicted PAR

Images were thresholded using ImageJ [20] to allow for quantification of the predicted leak (Figure 2). First, images were converted to greyscale 8 bit images and the level of background light (light transmitted through the annulus that was not blocked by the closed valve and aortic walls) was quantified. The threshold level was set at 130% of the background light level so that only unimpeded light passing between the aortic wall and closed valve (predicted PAR) was selected (Figure 2). Predicted extent of PAR was quantified as a percentage of the number of pixels within the thresholded leak divided by the number of pixels within the background projected annulus.

Analysis of Multiplanar Reformatted Images

Pre-procedure multiphase CT data sets were reconstructed at peak systolic phase (as detailed above) and loaded into dedicated cardiac image viewing software (Vitrea 6.7, Vital Images).

Multiplanar images were manipulated so that the annular plane -defined as the plane containing all three aortic cusp hinge points- was in the transverse plane, as previously reported. [17] The maximal diameter and orthogonal minimal diameter of the annulus were measured at this level.

Statistics

The chi squared test was used for comparisons of nominal data from the patient groups with and without PAR and results were reported as mean ± SD. A two-tailed p value of < 0.05 was considered to be statistically significant. Correlation between annulus measurements made on 2D data sets and 3D printed models was calculated using the Pearson correlation coefficient. The mean difference between the methods was calculated and plotted using a Bland Altman plot and 95% limits of agreement were reported (+/− 1.96 SD). Statistical analysis was performed using Prism 6 (Graph Pad, San Diego, CA).

RESULTS

Feasibility and Accuracy of 3D Printed Models

Segmentation time was approximately 10–30 minutes per model (Figure 1). Post-processing time using CAD software was approximately 10–30 minutes. Estimated printing time was 3.5 hours, and 3–4 aortic root models could be printed at one time. Post-print processing (removing support materials) took approximately 15–30 minutes Total production time from DICOM analysis to a final printed model was approximately 5 hours.

Patient-specific anatomy was preserved in the models as determined by visual assessment (Figure 3). This included overall size and shape of the annulus and LVOT and relationship of the coronary artery ostia to the annular plane. In addition, measurements of annulus minimum and maximum diameter made on printed 3D models were highly correlated with annulus measurements made from corresponding 2D image sets (Pearson correlation coefficient of 0.867). Measurements made on models closely agreed with traditional 2D measurements (mean difference of −0.34 mm, 95% limits of agreement ± 1.3 mm). (Figure 4)

3D printed models of valve prostheses were also highly accurate to within 0.1 mm of their designed dimensions (e.g within 0.1 mm of 23, 26 or 29 mm diameter) (Figure 2).

Light transmission test to predict paravalvular leaks

Using a light transmission test, 3D models correctly identified PAR in 6 of 9 patients and correctly excluded PAR in 5 of 7 patients (P=0.13 by Chi Square analysis) (Figure 5). The location of anticipated PAR (defined by clock-face position) was accurate, as 5 out of 6 were correctly anticipated within 2 clock face positions (Figure 6).

The 3 false-negative patients and 2 false-positive patients did not have obvious features that differentiated them from the correctly predicted cases, including valve size, valve type and whether re-ballooning was performed during placement (Table 1).

The predicted size of PAR was quantified as a percentage of total annulus area, but did not appear to correspond with the severity of PAR as detected on TTE. In the 2 false positive cases (no PAR), area of predicted PAR was 0.8 and 1.3%. In the 5 cases of mild PAR, predicted area ranged from 0.8–4.7%. In 1 case of moderate PAR, the predicted size was 1.0%.

DISCUSSION

The main findings of this study are: (i) 3D printed models provide a feasible, noninvasive technique to assist 3D visualization of patient-specific aortic root anatomy, and (ii) 3D modeling presents a novel opportunity to plan TAVR device placement *in situ*, and may complement traditional techniques used to predict and potentially avoid complications such as PAR.

A thorough understanding of a patient's aortic root anatomy is essential for appropriate device selection. Current imaging techniques convert a patient's 3D anatomy into a series of 2D images. 3D renderings can be created from this data and projected onto a 2D screen, but studies demonstrate that information is still lost to the observer in this format [21]. The creation of a physical 3D model may recapture some of this lost information and offers the opportunity to better visualize how complex patient anatomy will physically interact with implanted medical devices such as stents [6], occlusion devices [9], or prosthetic valves [6, 13, 15, 16].

Although most TAVR valves are round, the annulus is often more ellipse, and radial forces from the deployed valve can alter the resulting annulus shape. [22] In turn, variable forces from surrounding structures such as the septum and the left ventricular wall (in cases of LV hypertrophy) may affect the shape a deployed prosthetic valve ultimately takes. Different types of valves (e.g. the Edwards Sapien valve versus the Core valve) exert varying radial forces on the aortic root. [22] These physical interactions cannot be inferred from 2D images and are difficult to model in a virtual 3D space. Testing valves of different sizes and designs in a flexible 3D printed model may help to refine predictions of shape/ size mismatches by accounting for these physical interactions. Indeed, we were able to predict the presence of PAR in 6 of 9 patients by testing the fit of a valve model into aortic root models. Further, we were able to identify the location of PAR in 5 of 6 cases, suggesting that 3D models fitted with prosthetic valve models may help simulate how these structures interact with one another.

While promising, the prediction of PAR based on 3D models was far from optimal in this initial feasibility study. This is likely due, in part, to the fact that our current modeling technique did not incorporate important elements of the valvular complex (Table 2). For example, leaflets and leaflet calcium were not included in our models. Further, while we used flexible material to print the aortic root, this material does not match the true elastic modulus of the aortic wall—defined as the amount that a material will stretch or deform in response to force or stress.[23] Our printed 3D models were created from image data at peak systole, and therefore the dynamic nature of PAR across the cardiac cycle was not accounted for. For instance, it is possible that models created during diastole may enhance the ability to

visualize PAR. Finally, we used a 3D printed valve meeting the size specifications of the actual prosthetic valve, but our valve was made of hard plastic and was fixed in an expanded configuration. It is unknown whether the radial forces exerted by our valve model adequately mimicked that of the true valve prosthesis. Potential solutions to these design challenges are presented in Table 2.

Another possible source of error between predictions based on 3D models and actual PAR is an unforeseen procedural challenge, in particular valve positioning. In addition, because we used a valve in a fixed expanded position, we did not account for the ability to slightly under or over-distend the valve at placement, a technique that may allow for more precise sizing. However, a physical model does provide an opportunity to rehearse valve placement in a specific patient's aortic root and, in theory, may help operators anticipate some potential challenges.

The size of predicted PAR did not correlate with the actual severity of PAR. This may be partly due to the fact that the dynamic nature of a regurgitant jet across the cardiac cycle can lead to changes in overall size of PAR over time. Additionally, the size discrepancy could be due to inaccuracies of the light transmission test, where light reflected or refracted from the inner surface of the aortic model could change the shape of light recorded on film Despite this drawback, the light transmission test was a more robust assay in our hands than initial attempts to use water or sand with variable grain size to detect PAR.

The 2 false positive cases did not have any distinguishing features to explain why PAR was incorrectly predicted. In fact, it is noteworthy that there were not more false positives given the fact that valve leaflets were not included in our models. Calcifications on leaflets may, in some instances, seal gaps between the annulus and prosthesis as they are pushed out of the way by an expanding valve. It may be that loss of a portion of transmitted light due to reflection/refraction off the aortic wall during the light transmission test was helpful in compensating for the lack of displaced leaflets in the models.

In an era of precision and personalized medicine, physicians are increasingly tasked with considering each patient based on their unique anatomy. A major goal of this pilot study was to explore whether 3D printed models could predict PAR on an individual basis. Predictors of PAR such as annular and leaflet calcification and annulus shape perform well in larger studies [24–27], but may be less predictive for an individual patient than they are in a larger cohort. 3D printed models, while imperfect, were modestly accurate in predicting PAR on an individual basis. Understanding how to combine predictive information from both 2D and 3D data will likely lead to future improvements.

CONCLUSION

The use of pre-TAVR 3D printing provides a unique method to assess the physical interplay of the aortic root and implanted valves. With future optimization, including development of material that better reflects the mechanical properties of the aorta and associated calcium, this developing technology may help aid prediction of which patients are more likely to

develop PAR. Given these initial results, further studies focusing on both clinical application and 3D-printed model optimization are needed.

Acknowledgments

Sources of Support: Dr. Gonçalves receives funds from Portuguese Foundation for Science and Technology, Grant HMSP-ICS/007/2012

Abbreviations

PAR	paraaortic regurgitation
TAVR	transcatheter aortic valve replacement
3D	three-dimensional
STL	standard tessellation language
CCT	cardiac CT
TTE	transthoracic echocardiography

References

1. Himbert D, Vahanian A. Transcatheter Aortic Valve Replacement for Patients with Heart Failure. Heart Fail Clin. 2015; 11(2):231–242. DOI: 10.1016/j.hfc.2014.12.003 [PubMed: 25834972]
2. Kasel AM, Cassese S, Bleiziffer S, et al. Standardized imaging for aortic annular sizing: Implications for transcatheter valve selection. JACC Cardiovasc Imaging. 2013; 6(2):249–262. DOI: 10.1016/j.jcmg.2012.12.005 [PubMed: 23489539]
3. Yang T-H, Webb JG, Blanke P, et al. Incidence and Severity of Paravalvular Aortic Regurgitation With Multidetector Computed Tomography Nominal Area Oversizing or Undersizing After Transcatheter Heart Valve Replacement With the Sapien 3. JACC Cardiovasc Interv. 2015; 8(3): 462–471. DOI: 10.1016/j.jcin.2014.10.014 [PubMed: 25790764]
4. Généreux P, Head SJ, Hahn R, et al. Paravalvular leak after transcatheter aortic valve replacement: The new achilles' heel? A comprehensive review of the literature. J Am Coll Cardiol. 2013; 61(11): 1125–1136. DOI: 10.1016/j.jacc.2012.08.1039 [PubMed: 23375925]
5. Van Belle E, Juthier F, Susen S, et al. Postprocedural aortic regurgitation in balloon-expandable and self-expandable transcatheter aortic valve replacement procedures: Analysis of predictors and impact on long-term mortality: Insights from the France2 registry. Circulation. 2014; 129(13):1415–1427. DOI: 10.1161/CIRCULATIONAHA.113.002677 [PubMed: 24566199]
6. Wang H, Liu J, Zheng X, et al. Three-dimensional virtual surgery models for percutaneous coronary intervention (PCI) optimization strategies. Sci Rep. 2015 Jan.5:10945.doi: 10.1038/srep10945 [PubMed: 26042609]
7. Kim MS, Hansgen AR, Wink O, Quaife Ra, Carroll JD. Rapid prototyping: A new tool in understanding and treating structural heart disease. Circulation. 2008; 117(18):2388–2394. DOI: 10.1161/CIRCULATIONAHA.107.740977 [PubMed: 18458180]
8. Olivieri L, Krieger A, Chen MY, Kim P, Kanter JP. 3D heart model guides complex stent angioplasty of pulmonary venous baffle obstruction in a Mustard repair of D-TGA. Int J Cardiol. 2014; 172(2):e297–e298. DOI: 10.1016/j.ijcard.2013.12.192 [PubMed: 24447757]
9. Schmauss D, Haeberle S, Hagl C, Sodian R. Three-dimensional printing in cardiac surgery and interventional cardiology: a single-centre experience. Eur J Cardio-Thoracic Surg. 2014; :1–9. DOI: 10.1093/ejcts/ezu310

10. Mahmood F, Owais K, Montealegre-Gallegos M, et al. Echocardiography derived three-dimensional printing of normal and abnormal mitral annuli. Ann Card Anaesth. 2014; 17(4): 279.doi: 10.4103/0971-9784.142062 [PubMed: 25281624]
11. Binder TM, Moertl D, Mundigler G, et al. Stereolithographic biomodeling to create tangible hard copies of cardiac structures from echocardiographic data: In vitro and in vivo validation. J Am Coll Cardiol. 2000; 35(1):230–237. DOI: 10.1016/S0735-1097(99)00498-2 [PubMed: 10636285]
12. Witschey WRT, Pouch AM, McGarvey JR, et al. Three-Dimensional Ultrasound-Derived Physical Mitral Valve Modeling. Ann Thorac Surg. 2014; 98(2):691–694. DOI: 10.1016/j.athoracsur.2014.04.094 [PubMed: 25087790]
13. Dankowski R, Baszko A, Sutherland M, et al. 3D heart model printing for preparation of percutaneous structural interventions: description of the technology and case report. Kardiol Pol. 2014; 72(6):546–551. DOI: 10.5603/KP.2014.0119 [PubMed: 24961451]
14. Díaz Lantada A, Valle-Fernández R Del, Morgado PL, et al. Development of personalized annuloplasty rings: Combination of CT images and CAD-CAM tools. Ann Biomed Eng. 2010; 38(2):280–290. DOI: 10.1007/s10439-009-9805-z [PubMed: 19826955]
15. Poterucha JT, Foley TA, Taggart NW. Percutaneous pulmonary valve implantation in a native outflow tract: 3-dimensional DynaCT rotational angiographic reconstruction and 3-dimensional printed model. JACC Cardiovasc Interv. 2014; 7(10):e151–e152. DOI: 10.1016/j.jcin.2014.03.015 [PubMed: 25341717]
16. Armillotta A, Bonhoeffer P, Dubini G, et al. Use of rapid prototyping models in the planning of percutaneous pulmonary valved stent implantation. Proc Inst Mech Eng H. 2007; 221(4):407–416. [PubMed: 17605398]
17. Achenbach S, Delgado V, Hausleiter J, Schoenhagen P, Min JK, Leipsic Ja. SCCT expert consensus document on computed tomography imaging before transcatheter aortic valve implantation (TAVI)/transcatheter aortic valve replacement (TAVR). J Cardiovasc Comput Tomogr. 2012; 6(6):366–380. DOI: 10.1016/j.jcct.2012.11.002 [PubMed: 23217460]
18. Pibarot P, Hahn RT, Weissman NJ, Monaghan MJ. Assessment of Paravalvular Regurgitation Following TAVR. JACC Cardiovasc Imaging. 2015; 8(3):340–360. DOI: 10.1016/j.jcmg.2015.01.008 [PubMed: 25772838]
19. Goncalves A, Almeria C, Marcos-alberca P, et al. THREE-DIMENSIONAL ECHOCARDIOGRAPHY : NOVEL USES Three-Dimensional Echocardiography in Paravalvular Aortic Regurgitation Assessment after Transcatheter Aortic Valve Implantation. J Am Soc Echocardiogr. 2012; 25(1):47–55. DOI: 10.1016/j.echo.2011.08.019 [PubMed: 21962448]
20. Rasband, WS. p. 1997-2014.No Title. http://imagej.nih.gov/ij/
21. Rojas GM, Gálvez M, Vega Potler N, et al. Stereoscopic three-dimensional visualization applied to multimodal brain images: clinical applications and a functional connectivity atlas. Front Neurosci. 2014 Nov.8:1–14. DOI: 10.3389/fnins.2014.00328 [PubMed: 24478622]
22. Litmanovich DE, Ghersin E, Burke Da, Popma J, Shahrzad M, Bankier Aa. Imaging in Transcatheter Aortic Valve Replacement (TAVR): Role of the radiologist. Insights Imaging. 2014; 5(1):123–145. DOI: 10.1007/s13244-013-0301-5 [PubMed: 24443171]
23. Khanafer K, Duprey A, Zainal M, Schlicht M, Williams D, Berguer R. Determination of the elastic modulus of ascending thoracic aortic aneurysm at different ranges of pressure using uniaxial tensile testing. J Thorac Cardiovasc Surg. 2011; 142(3):682–686. DOI: 10.1016/j.jtcvs.2010.09.068 [PubMed: 21616506]
24. Wong DTL, Hons M, Bertaso AG, et al. Relationship of aortic annular eccentricity and paravalvular regurgitation post transcatheter aortic valve implantation with CoreValve. J Invasive Cardiol. 2013; 25(4):190–195. http://www.ncbi.nlm.nih.gov/pubmed/23549493. [PubMed: 23549493]
25. Pavicevic J, Nguyen TDL, Caliskan E, et al. Aortic valve calcium score is a significant predictor for the occurrence of post-interventional paravalvular leakage after transcatheter aortic valve implantation — Results from a single center analysis of 260 consecutive patients. Int J Cardiol. 2015; 181:185–187. DOI: 10.1016/j.ijcard.2014.12.032 [PubMed: 25528309]

26. Buellesfeld L, Stortecky S, Heg D, et al. Extent and distribution of calcification of both the aortic annulus and the left ventricular outflow tract predict aortic regurgitation after transcatheter aortic valve replacement. EuroIntervention. 2014; 10(6):732–738. [PubMed: 25330505]

27. Azzalini L, Ghoshhajra BB, Elmariah S, et al. The aortic valve calcium nodule score (AVCNS) independently predicts paravalvular regurgitation after transcatheter aortic valve replacement (TAVR). J Cardiovasc Comput Tomogr. 2014; 8(2):131–140. DOI: 10.1016/j.jcct.2013.12.013 [PubMed: 24661826]

28. Tymrak BM, Kreiger M, Pearce JM. Mechanical properties of components fabricated with open-source 3-D printers under realistic environmental conditions. Mater Des. 2014; 58:242–246.

- 3D printing can provide graspable models of patient-specific anatomy for TAVR planning.
- 3D aortic root models were successfully printed from preoperative CCT and were highly accurate.
- A light transmission test was designed to assess fit of valves within 3D printed aortic root models.
- Paravalvular regurgitation was correctly predicted in 6 of 9 patients and ruled out in 5 of 7 patients.
- With optimization, 3D models may one day complement traditional techniques used for predicting PAR.

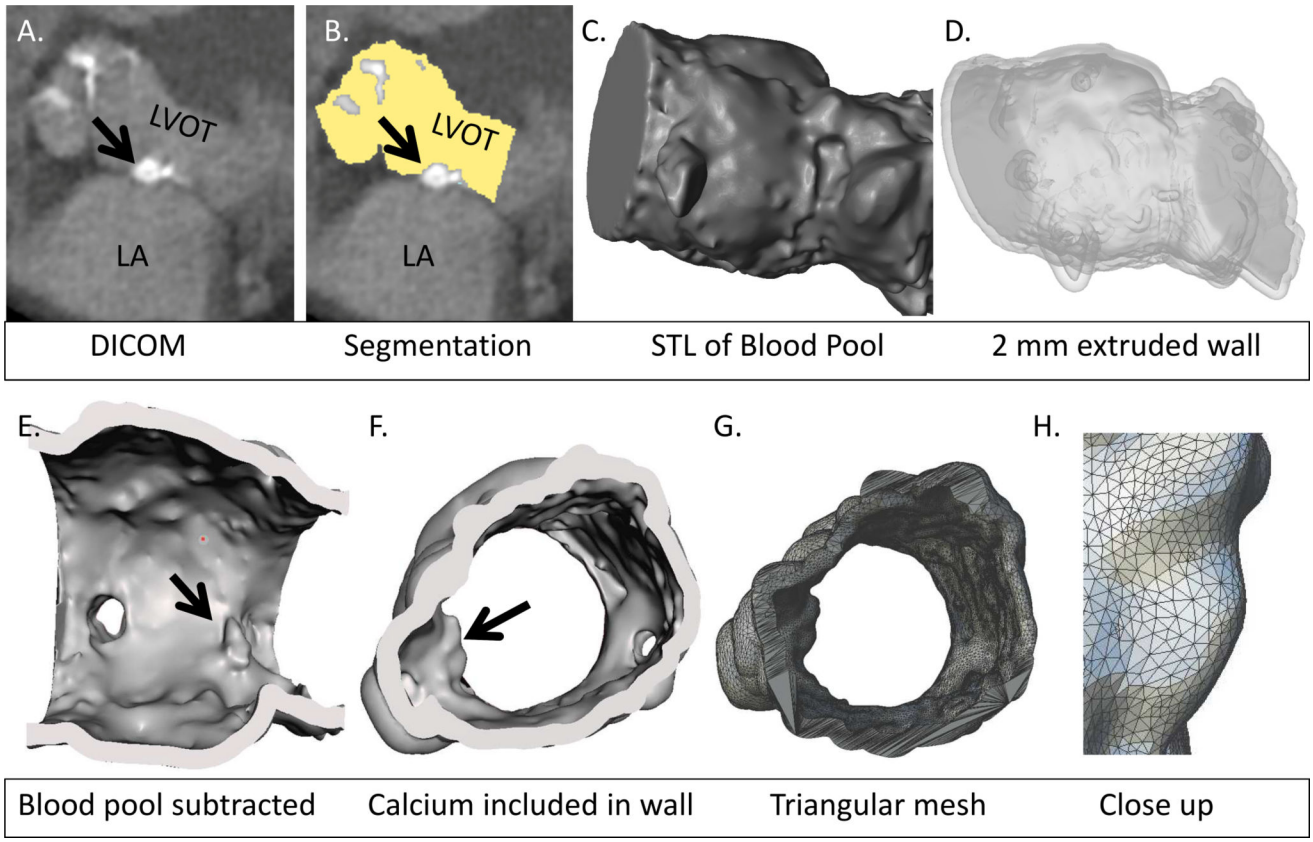

Figure 1. Creation of STL files from DICOM Images

A. STL files were created from standard CT DICOM image data sets. Note annular calcification (black arrow) extending from the mitral annulus. B. The blood pool was segmented using a combination of threshold and manual segmentation. In this example, the contrast opacification is not ideal, but was still adequate for printing. Again, note the annular calcification which is excluded in the segmentation based on its higher Hounsfield unit value. C. Segmentation data was converted to an STL file and exported into CAD software for further processing. At this point, the model is simply the segmented blood pool. Note the indentation from the excluded calcification (white arrow). D. To create a lumen, a 2 mm thick wall was extruded outwards in all directions from the blood pool. This preserved the integrity of the inner lumen data and allowed for a wall thickness suitable for printing. E. After extrusion, the blood pool was subtracted, leaving just the wall. Note that the calcification is now represented as a positive shape (black arrow). G. Visualization of the triangular mesh that defines the printable object. H. Close up view allows more detailed depiction of the triangle mesh. LVOT = Left ventricular outflow track. LA = Left Atrium

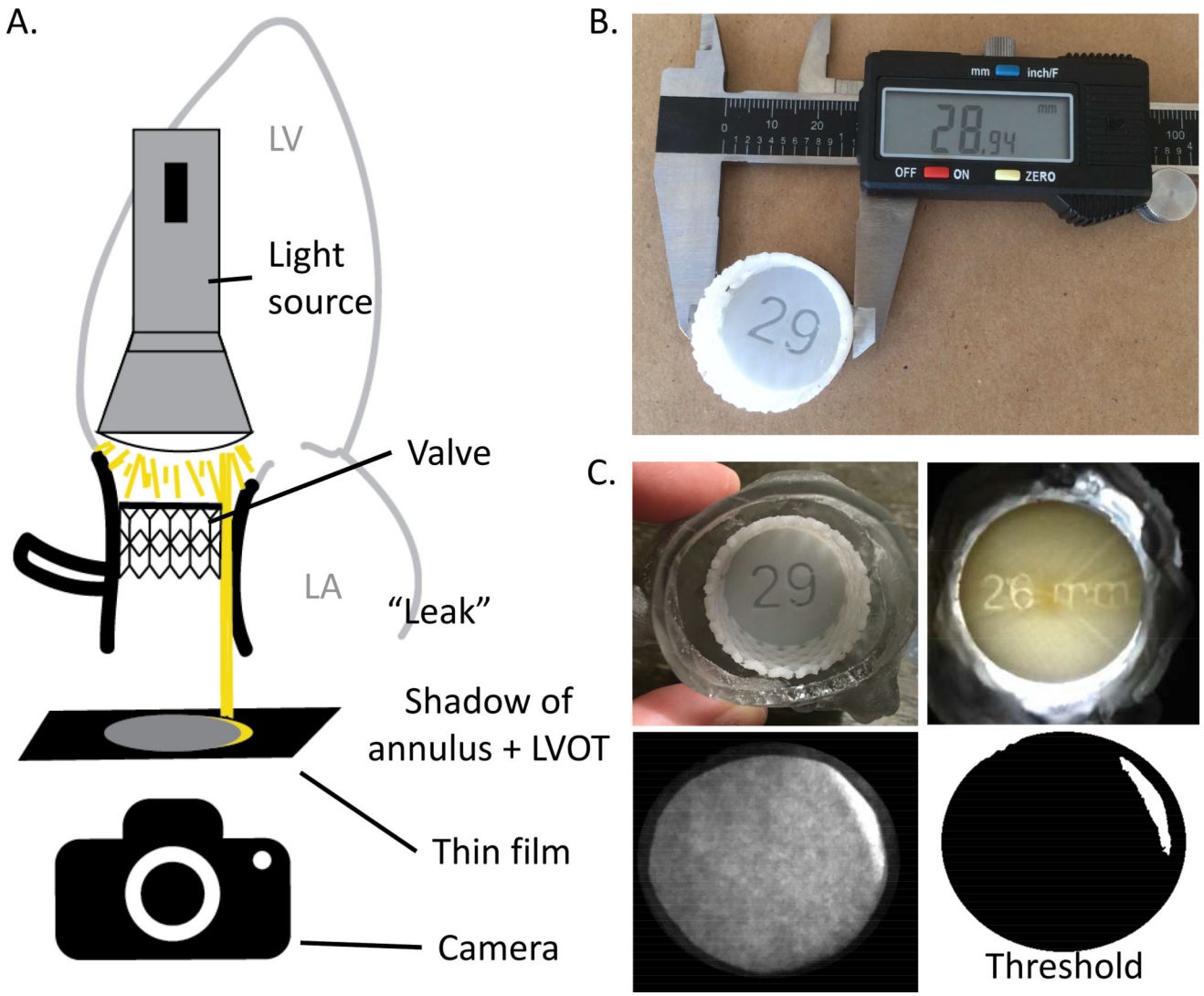

Figure 2. A simple light transmission experiment designed to predict paravalvular leaks

A. Illustration depicting experimental set-up. A valve was placed into the 3D printed aortic valve complex at the level of the annulus and a light was focused on the left ventricular side of the printed valve. Light was almost completely blocked by the opaque closed bottom of the valve, allowing a very faint light in the shape of the annulus and proximal LVOT to project onto the thin film. However, unimpeded light was able to pass through any gaps between the aortic annulus and the valve and was detected by a digital camera positioned on the aortic side of the valve. B. 3D printed valve designed to the specifications of the Edwards Sapien Valve. C. Upper left panel: 3D printed valve situated in a 3D printed aortic root. Upper right panel: Light focused on the LVOT side of the valve passes through cracks between an ill-fitting 26 mm valve. Bottom left panel: example of light projected onto a thin film. The grey color reflects the shadow of the annulus and proximal LVOT. The bright white crescent reflects unimpeded light hitting the thin film. Bottom right panel: Thresholded image for quantification purposes.

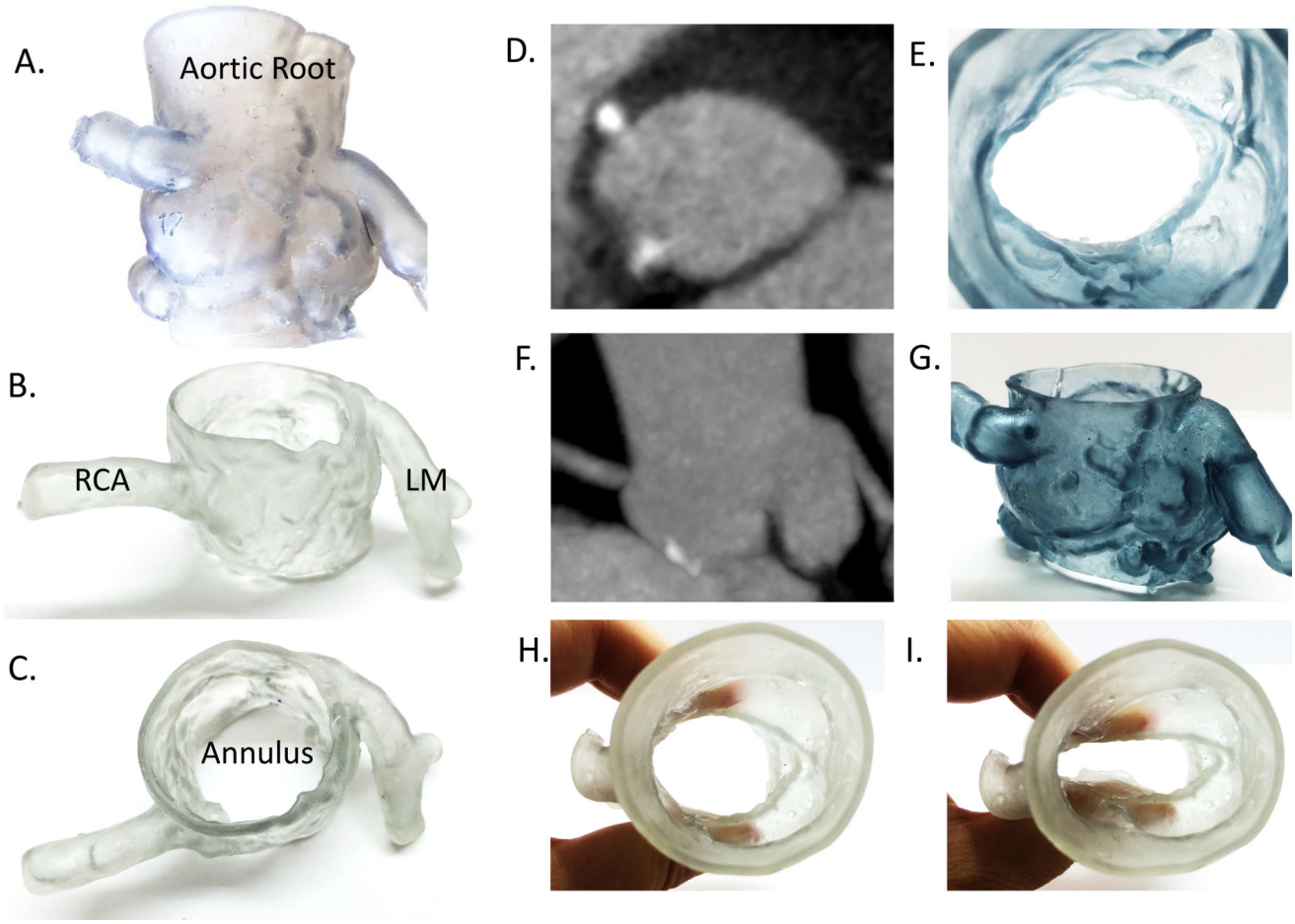

Figure 3. 3D printed models of the aortic root accurately depict morphology

A-C. 3D printed aortic valve complexes from two different patients demonstrating anatomy included in the models. RCA: right coronary artery. LM: left main artery. D-E. 3D printed model from an individual patient (E) reproduces the geometry of the annulus as seen on CT (D). F-G. 3D printed model from another patient (G) reproduces the geometry of the sinuses of Valsalva and coronary artery take-offs as seen on CT (F). H-I. 3D models were printed in flexible material to mimic the elastic properties of the aorta.

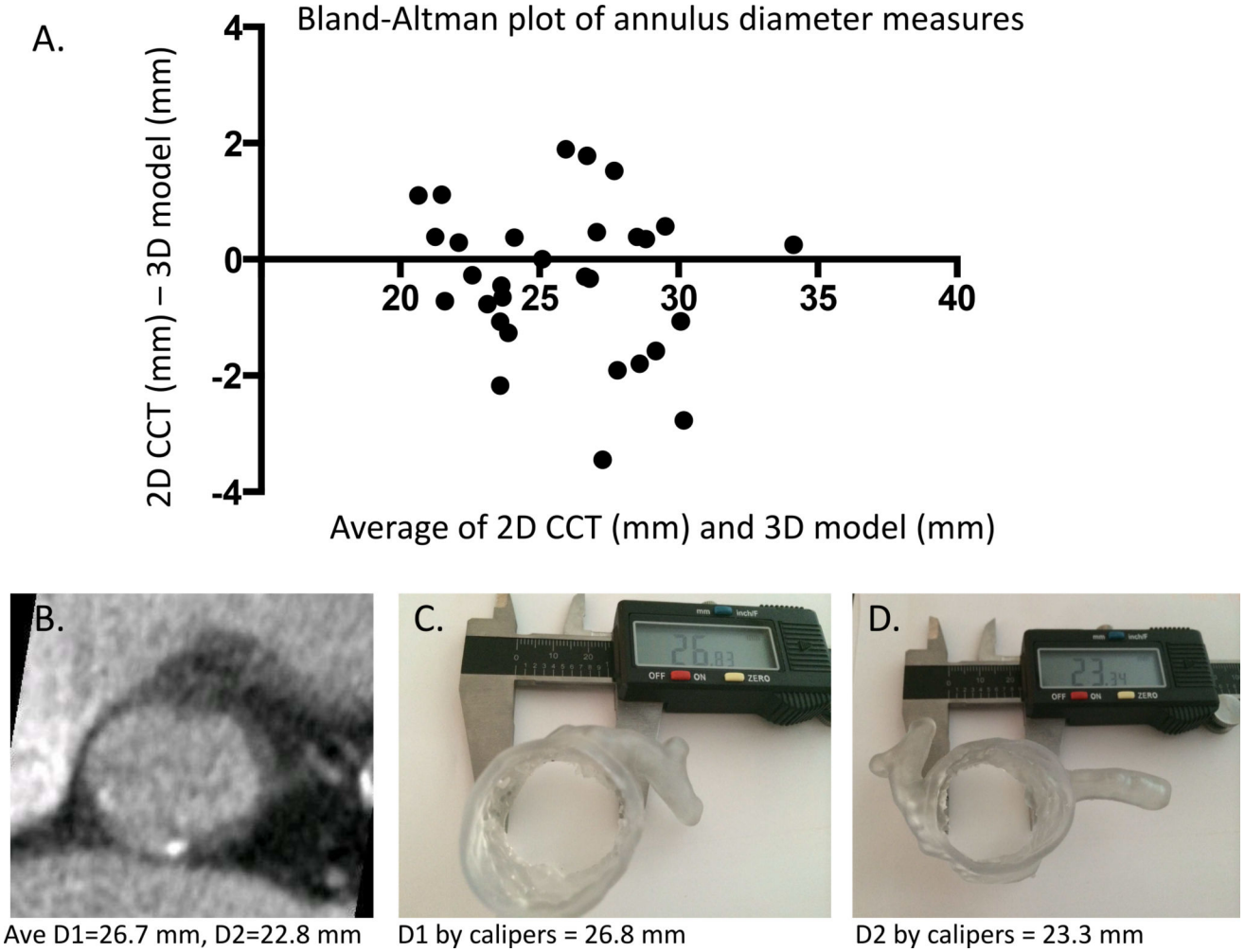

Figure 4. 3D models accurately depict annulus size

A. Bland-Altman plot of annulus measurements made on 2D and physical 3D data sets. The difference between measurements made on 2D CT and 3D printed models is plotted against an average of the 2 measurements. The fact that the points lie around the 0 line demonstrates that there is no inherent bias between the two methods. B. CT multiplanar reformat at the annular plane. Maximum and minimum diameter are stylistically depicted with white lines, with actual data reported below the image (average from 2 separate readers). C. Maximum diameter of the same patient as in B was measured with calipers. A separate set of models was printed with a cut made at the annular plane to facilitate physical measurements without manipulating or deforming the flexible models. D. Minimum diameter measured in the same patient.

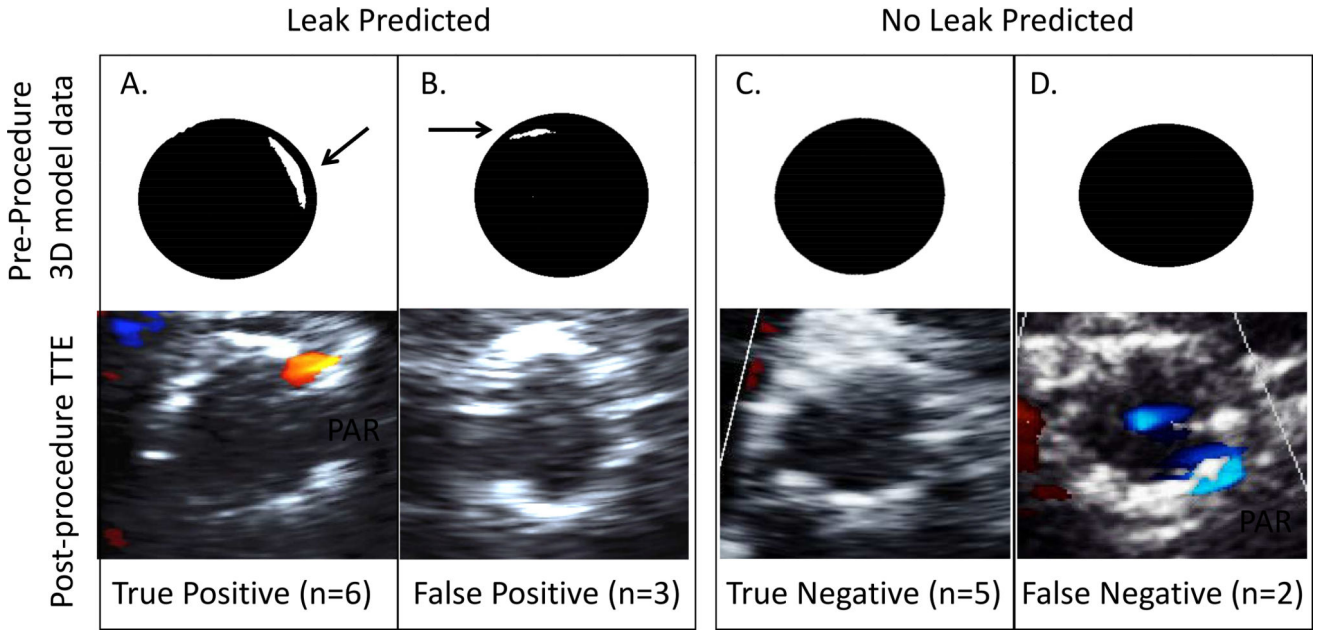

Figure 5. Predicted PAR vs. Actual PAR Demonstrated by TTE

A. Example of correctly predicted PAR. Top panel: Threshold image demonstrates PAR predicted by the light transmission test. Bottom panel: Post-procedure TTE data demonstrates PAR. B. Example of a false positive prediction. Top panel: PAR is predicted at the 11:00 position. Bottom panel: TTE confirms absence of PAR. C. Example of a true negative. Top panel: no PAR is predicted by the light transmission test. Bottom panel: TTE confirms absence of PAR. D. Example of a false negative prediction. Top panel: no PAR is predicted by the light transmission test. Bottom panel: TTE confirms the presence of PAR.

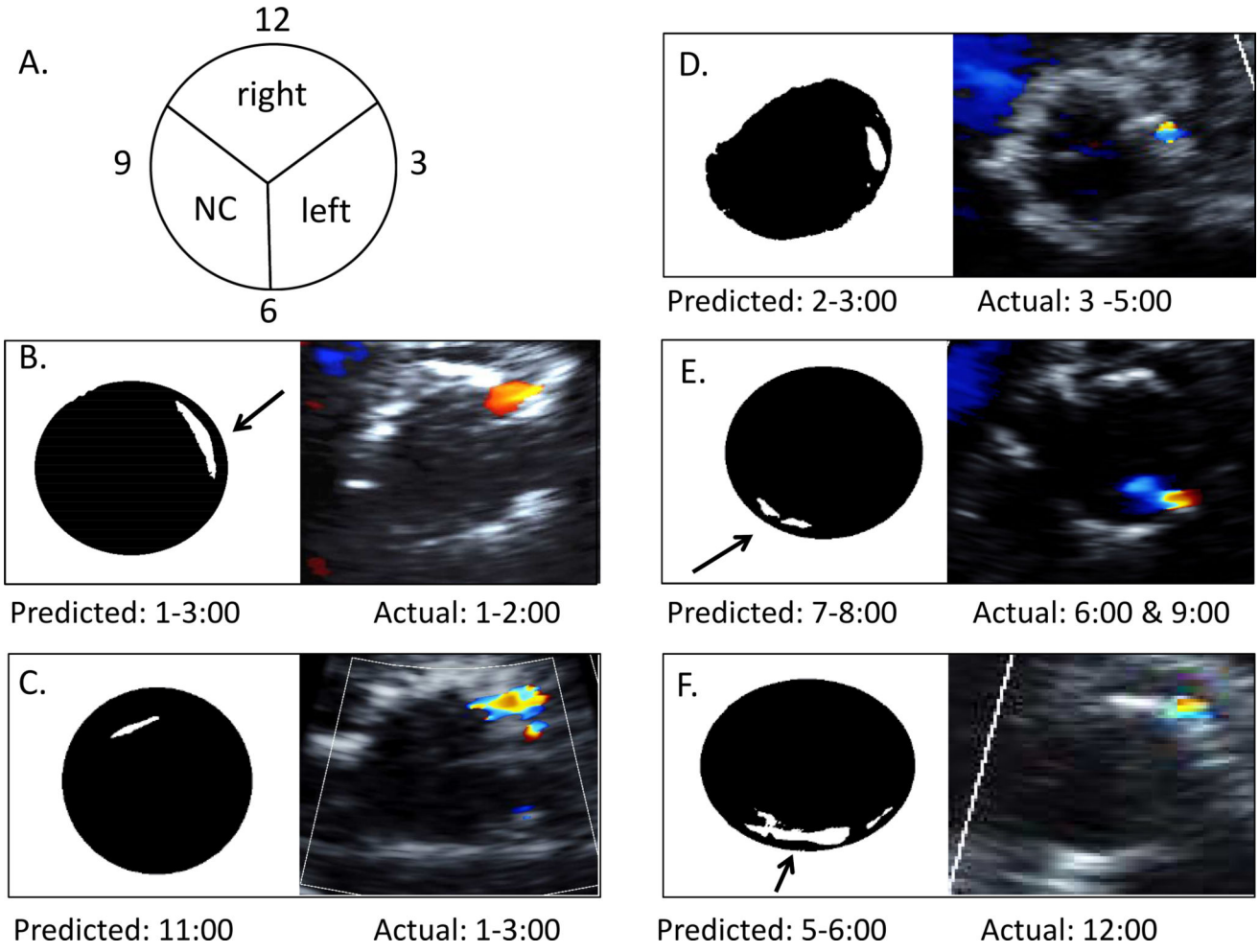

Figure 6. Predicted vs. actual clock face position of PAR

A. Clock face scheme for describing position of PAR, adapted from Goncalves et al.[19] B-E. Left-hand panels demonstrate the predicted PAR position based on the 3D printed models and light transmission experiment. Right-hand panels are representative post-procedure TTE images demonstrating actual position of PAR. All predicted and actual TTE data are oriented according to the clock face scheme demonstrated in A. F. The left-hand panel demonstrates the most incorrect prediction in the group, off by roughly 6 clock face positions.

Table 1

PAR	Predicted leak? [amount] (Location)	PAR severity (location)	Approach	Valve Size (mm)	Gender	Age, yrs	Valve type	Re-ballooned?	Annular calcs? (visual grades for sectors)
+	*No*	*Moderate (5:00)*	*femoral*	*26*	*F*	*74*	*Commercial Sapien*	*Yes*	*Yes (1,2,0)*
+	*No*	*Mild (6:00)*	*apical*	*29*	*M*	*85*	*Sapien XT*	*No*	*Yes (2,1,0)*
+	*No*	*Mild (6:00–8:00)*	*apical*	*26*	*F*	*79*	*Commerical Sapien*	*Yes*	*Yes (0,0,1)*
+	Yes [3%] (1:00–3:00)	Mild (1:00–2:00)	femoral	26	M	87	Commercial Sapien XT	Yes	No (0,0,0)
+	Yes [1%] (11:00)	Moderate (1:00–3:00)	femoral	26	F	74	Sapien 3	Yes	Yes (0,2,0)
+	Yes [2.6%] (2:00–3:00)	Mild (3:00–5:00)	aortic	26	M	79	Commercial Sapien	No	No (0,0,0)
+	Yes [0.8%] (10:00–11:00)	Mild (12:00)	femoral	29	M	88	Sapien XT	No	No (0,0,0)
+	Yes [1.3%] (7:00–8:00)	Mild (6:00 & 9:00)	femoral	29	M	85	Sapien 3	Yes	No (0,0,0)
+	Yes [4.7%] (5:00–7:00)	Mild (12:00)	femoral	26	M	69	Sapien 3	No	No (0,0,0)
−	*Yes [0.8%] (8:00)*	*None*	*femoral*	*26*	*M*	*89*	*Commercial Sapien*	*No*	*Yes (0,1,2)*
−	*Yes [1.3%] (6:00)*	*None*	*aortic*	*26*	*M*	*89*	*Commercial Sapien*	*No*	*No (0,0,0)*
−	No	None	femoral	23	F	91	Commercial Sapien	No	No (0,0,0)
−	No	None	femoral	26	M	78	Sapien 3	Yes	Yes (0,2,2)
−	No	None	aortic	29	M	86	Sapien 3	No	Yes (0,1,0)
−	No	None	aortic	26	F	77	Commercial Sapein	No	Yes (0,1,2)
−	No	None	femoral	29	M	87	Sapien XT	No	No (0,0,0)

Legend: Column 1. PAR: para-aortic regurgitation. + indicates patients with confirmed PAR, while − indicates patients without PAR. In column 2, quantification of predicted PAR is reported as a percentage of the total area of the annulus and is indicated in [brackets]. The predicted clock face position is reported in (parentheses). In column 9, re-ballooned refers to cases where the interventionalist chose to balloon open the TAVR valve twice during the placement of the valve. This was done at the discretion of the interventionalist. In column 10, the presence or absence of annular calcifications is reported, and is graded as grade 0, no calcification; grade 1, small (< 1 mm) non-protruding calcification; grade 2, calcium protruding > 1mm into the annulus or extensive (> 50% of cusp sector) calcification; grade 3, protruding calcium (> 1mm) and extensive (> 50% of cusp sector) calcification. Grades are reported in the order (right coronary sector, left coronary sector, noncoronary sector).

Table 2

"Wish List" For 3D Models of the Aortic Root Used for TAVR Planning

Wanted Feature	Current Challenge	Potential Solution
Valve leaflets	- Motion causes leaflet blurring. - Leaflets are often too thin to accurately segment.	- Improved temporal resolution will result in less motion. - Obtaining imaging during diastole minimizes leaflet motion. - If valves are calcified, the calcification can be segmented and the leaflet shape inferred.
Calcification hardness similar to actual calcium	- Many printers currently do not have the capability to print multiple materials, and those that do tend to be more expensive.	- Wider availability of more affordable printers with multi-material capability.
Material matching the properties of the aortic wall, such as deformability secondary to external forces (elastic modulus)	- The elastic modulus of the aorta varies based on wall thickness, disease state and aneurysmal dilation, making it difficult to predict on an individual basis; however, it is roughly between 3–9 MPa [25]. - Many widely available materials do not match the elastic modulus of the aorta, with ABS in the 1400–3100 MPa range and PLA in the 4000 MPa range [28].	- Many printing materials have a published elastic modulus. - Rubber materials are in the general range of the aorta (0.1–10 MPa) - Ongoing development of new materials.
Actual prosthetic valves	- Prosthetic valves are expensive; it is not feasible to use actual valves for routine pre-surgical planning.	- A stand-in mock up of a valve that has the same dimensions and elastic modulus and which applies the same radial forces as the true valve.

Abbreviations. ABS: Acrylonitrile butadiene styrene. PLA: polylactic acid. MPa: megapascal, units for elastic modulus.